HHS Public Access

Author manuscript

Clin Cancer Res. Author manuscript; available in PMC 2016 December 01.

Published in final edited form as:

Clin Cancer Res. 2015 December 1; 21(23): 5277–5285. doi:10.1158/1078-0432.CCR-15-0552.

A Phase I/II Study for Analytic Validation of ^{89}Zr-J591 ImmunoPET as a Molecular Imaging Agent for Metastatic Prostate Cancer

Neeta Pandit-Taskar[1,2,*], **Joseph A. O'Donoghue**[3], **Jeremy C. Durack**[1], **Serge K. Lyashchenko**[4,5], **Sarah M. Cheal**[1,4], **Volkan Beylergil**[1], **Robert A. Lefkowitz**[2], **Jorge A. Carrasquillo**[1,2], **Danny F. Martinez**[6], **Alex Mak Fung**[1], **Stephen B. Solomon**[1,2], **Mithat Gonen**[7], **Glenn Heller**[7], **Massimo Loda**[8], **David M. Nanus**[9], **Scott T. Tagawa**[9], **Jarett L. Feldman**[6], **Joseph R. Osborne**[1,2], **Jason S. Lewis**[2,4,5], **Victor E. Reuter**[10], **Wolfgang A. Weber**[1,2], **Neil H. Bander**[9,11], **Howard I. Scher**[6,9], **Steven M. Larson**[1,2,4,**], and **Michael J. Morris**[6,9,**]

[1] Department of Radiology, Memorial Sloan Kettering Cancer Center, New York, New York.

[2] Department of Radiology, Weill Cornell Medical College, New York, New York.

[3] Department of Medical Physics, Memorial Sloan Kettering Cancer Center, New York, New York.

[4] Molecular Pharmacology and Chemistry Program, Memorial Sloan Kettering Cancer Center, New York, New York.

[5] Radiochemistry and Molecular Imaging Probe Core Facility, Memorial Sloan Kettering Cancer Center, New York, New York.

[6] Department of Medicine, Memorial Sloan Kettering Cancer Center, New York, New York.

[7] Department of Biostatistics, Memorial Sloan Kettering Cancer Center, New York, New York.

[8] Dana-Farber Cancer Institute; Brigham & Women's Hospital; and Broad Institute, Boston, Massachusetts.

[9] Department of Medicine, Weill Cornell Medical College, New York, New York.

[10] Department of Pathology, Memorial Sloan Kettering Cancer Center, New York, New York.

[11] Department of Surgery, Memorial Sloan Kettering Cancer Center, New York, New York.

Abstract

Purpose—Standard imaging for assessing osseous metastases in advanced prostate cancer remains focused on altered bone metabolism and is inadequate for diagnostic, prognostic, or predictive purposes. We performed a first-in-human phase I/II study of ^{89}Zr-DFO-huJ591 (^{89}Zr-

[*]Corresponding Author: Neeta Pandit-Taskar, MD Molecular Imaging and Therapy Service, Department of Radiology Memorial Sloan Kettering Cancer Center, 1275 York Avenue, Box 77 New York, NY 10065 Tel: 212-639-3046; Fax: 212-717-3268; pandit-n@mskcc.org.

[**]Joint senior authors

Conflict of interest disclosure: The authors report no actual or potential conflict of interest regarding any financial, personal, or other relationships with other individuals or organizations that could inappropriately influence the research described in this manuscript.

J591) PET/CT immunoscintigraphy to assess performance characteristics for detecting metastases compared to conventional imaging modalities (CIMs) and pathology.

Experimental Design—Fifty patients with progressive metastatic castration-resistant prostate cancers were injected with 5 mCi of ^{89}Zr-J591. Whole body PET/CT scans were obtained, and images were analyzed for tumor visualization. Comparison was made to contemporaneously obtained bone scintigraphy and cross-sectional imaging on a lesion-by-lesion basis, and with biopsies of metastatic sites.

Results—Median standardized uptake value for ^{89}Zr-J591-positive bone lesions (n = 491) was 8.9; soft tissue lesions (n = 90): 4.8 ($p < .00003$). ^{89}Zr-J591 detected 491 osseous sites compared to 339 by MDP, and 90 soft tissue lesions compared to 124 by CT. Compared to all CIMs combined, ^{89}Zr-J591 detected an additional 99 osseous sites. Forty-six lesions (21 bone, 25 soft tissue) were biopsied in 34 patients; 18/19 ^{89}Zr-J591-positive osseous sites and 14/16 ^{89}Zr-J591-positive soft tissue sites were positive for prostate cancer. The overall accuracy of ^{89}Zr-J591 was 95.2% (20/21) for osseous lesions and 60% (15/25) for soft tissue lesions.

Conclusions—^{89}Zr-J591 imaging demonstrated superior targeting of bone lesions relative to CIMs. Targeting soft tissue lesions was less optimal, although ^{89}Zr-J591 had similar accuracy as individual CIMs. This study will provide benchmark data for comparing performance of proposed PSMA targeting agents for prostate cancer.

Keywords

^{89}Zr-J591; J591 antibody; radioimmunoscintigraphy; prostate cancer; lesion detection

INTRODUCTION

The lack of imaging methods to directly visualize metastatic prostate cancer poses a challenge to staging, prognostication, and assessing treatment response of men with metastatic disease. Bone scintigraphy, the most common standard imaging modality for the evaluation of bone metastasis, is highly sensitive; however, it is also very nonspecific. The methylenediphosphonate bone scan (MDP) demonstrates reactive bone deposition but not cancer itself. Because many benign conditions may simulate tumor and therapeutic changes are not detectable early, and since regression and progression are indistinguishable, the practical use of MDP is somewhat limited. Additionally, bone lesions as seen on computerized tomography (CT) and plain radiographs generally appear as sclerotic lesions and are unrelated to active tumor size; CT scans also cannot differentiate between the healing effects of therapy versus osteoblastic activity due to true disease progression. ^{18}F-flourodeoxyglucose (FDG) PET imaging, while it reflects increased glucose metabolism of more aggressive disease in prostate cancer patients, has low sensitivity (1-6).

Accurate imaging modalities are therefore needed in order to develop imaging biomarkers, whether used for prognosis, prediction, or as surrogates for clinical effects. Additionally, without the ability to image the cancer directly, the acquisition of metastatic tissue for study and diagnostic purposes is impeded.

In order to overcome these limitations, we are developing an imaging biomarker for prostate cancer that is tumor-directed and quantifiable. PSMA (prostate-specific membrane antigen) is a peptidase widely expressed by primary and metastatic prostate cancer (7, 8). Several imaging probes based on intact PSMA antibodies, antibody fragments, and small molecule PSMA inhibitors have shown great promise for imaging prostate cancer with SPECT and PET (9-25). While a number of other tracers have been used for assessment of disease in prostate cancer, thus far none have been validated in controlled clinical trials for routine clinical use (9-16).

A humanized monoclonal antibody, huJ591 (J591) targets the extracellular domain of PSMA (17-20). Imaging of metastatic disease with ^{111}In-J591 and ^{177}Lu-J591 in prostate cancer and other tumors has been reported (21-24). More recently, we have developed and characterized ^{89}Zr-DFO-huJ591 (^{89}Zr-J591) (25) for PET imaging of PSMA-expressing cancers. We conducted a first-in-human study of ^{89}Zr-J591 in metastatic prostate cancer and have previously reported on the safety, biodistribution, and pharmacokinetics of imaging with ^{89}Zr-J591 in prostate cancer patients (21, 26). This study is an assessment of ^{89}Zr-J591 as an imaging biomarker, and represents the analytic validation of the biomarker as it assesses the performance characteristics of the tracer, using standard imaging modalities and biopsy specimens as comparators.

MATERIALS AND METHODS

This was a phase I/II prospective study of ^{89}Zr-J591in metastatic, castration-resistant prostate cancer (mCRPC). The primary endpoints were to determine the safety, biodistribution, and tumor localization of ^{89}Zr-J591. Secondarily, it compared ^{89}Zr-J591 PET lesion detection with that of conventional imaging and tissue biopsies. Patients with progressive, histologically confirmed prostate cancer were eligible. Progression was defined as a new lesion on bone scan or an increase in measurable soft tissue disease or new sites of soft tissue disease detected by CT scan or MRI. Biochemical progression was defined as a minimum of three rising PSA values from baseline with a minimum percentage increase of 25%. Additional eligibility criteria included a performance status of 60 or higher on the Karnofsky Performance Status (KPS) and adequate hepatic function. All patients underwent FDG PET within two weeks, and MDP and CT scan within four weeks prior to ^{89}Zr-J591 imaging. Patients with PSMA-positive cancers underwent no screening.

Antibody injection

The J591 was chelated with desferrioxamine-p-SCN (DFO) and subsequently radiolabeled with ^{89}Zr, using previously described methodology (27) and as detailed in our prior publication (26). The mean activity administered was 5.5.1 +/− 0.4 mCi and the mean amount of the radiolabeled J591 administered was 1.7 mg. All injections were co-administered with cold huJ591 antibody for a total antibody dose of 25 mg; this dose was chosen based on prior studies that showed saturation of liver at 25 mg dose (23). The cold antibody was delivered intravenously over 5 minutes, followed immediately by a 1-minute infusion of the radiolabeled antibody. No pre-medications were administered to initial patients; however, due to minor grade I reactions of chills or rigors seen in a small number

of patients, subsequent patients (n = 15) were premedicated with acetaminophen (500 mg) and Benadryl (25 mg).

PET imaging

Patients underwent PET scans extending from vertex to mid-thighs. In patients where skeletal disease in lower limbs was known to be present per conventional imaging, the scan was extended to include the thighs and entire legs. Four scans were performed on the first 10 patients at the following time points: 2-4 hours on the day of infusion, ~24 h, 48-120 h, and 144-168 h. The remaining 40 patients were imaged 6-8 days after the antibody injection, based on the initial analysis indicating the best target-to-background ratios at that time point. All scans were performed on the same scanner (GE Discovery DSTE) in 3D mode with 7 min/FOV at day 6-8. Images were constructed using iterative reconstruction and attenuation correction.

Image interpretation and lesion detection

Lesion uptake with ^{89}Zr-J591 was evaluated using the last imaging time day 6-8 for all 50 patients. For each patient, whole body images were visually and semi-quantitatively analyzed. Foci of increased uptake were graded on a scale of 1-5 (1 = negative, 2 = probably negative, 3 = equivocal, 4 = probably positive, 5 = definitely positive). Lesions graded 4 and 5 were considered positive. Equivocal uptake was further classified as positive or negative by consensus of three nuclear medicine readers (NPT, JAC, and SML). Intensity of uptake was quantified by maximum standardized uptake values (SUVmax) for multiple lesions in a patient. Baseline FDG, CT scans, and ^{99m} Tc-MDP bone scans were reviewed for lesions by nuclear medicine physicians and radiologists who were blinded to the other imaging results. All lesions detected by each modality were recorded separately.

Lesion biopsy

Up to two lesions (one bone and one soft tissue lesion, wherever feasible) were biopsied in patients who consented to biopsy, obtained within four weeks following ^{89}Zr-J591 imaging. The lesions most preferred for biopsy were those that had uptake on ^{89}Zr-J591 imaging or suspicious on all or most imaging modalities. The final biopsy site was decided in consultation with the Interventional Radiology service for feasibility.

Image analysis

We implemented an analysis plan comprising four elements: 1) All detectable sites of disease by all modalities were graded by separate readers; 2) Each detectable lesion site on ^{89}Zr-J591 imaging was compared with standard imaging on a site-by-site basis, including ^{99m}Tc bone scan for bone lesions and CT scanning (limited cases with MRI as described in methods) for soft tissue lesions; 3) Pathology of image-directed biopsy tissue sites was compared to imaging findings; and 4) For all non-biopsied sites of ^{89}Zr-J591 imaging, follow-up imaging performed for clinical reasons was evaluated to determine the presence or absence of disease at the site of uptake.

The concordance between ^{89}Zr-J591 and MDP was determined by plotting the number of lesions detected by ^{89}Zr-J591 scan versus MDP for each of the 50 patients.

Statistical methods

This prospective study was designed with the objective of evaluating the ability of ^{89}Zr-J591 to detect known sites of disease. Since no gold standard is available, a known site of disease was defined in the protocol as any lesion that was identified by conventional imaging methods at baseline. This does not lend itself to accurate estimation of specificity, so the protocol focused on the estimation of sensitivity using all sites identified by conventional imaging as the denominator. Assuming an intra-patient correlation of 0.1 (based on our experience of FDG PET in this disease), the estimate of sensitivity was projected to be within ±9% of its true value if we accrued 50 patients, assuming that the true sensitivity is 50%. If the sensitivity is higher, then our estimates will be more precise. Soft tissue lesions and bone lesions were treated separately.

We also used an emerging methodology to predict the number of positive lesions among the non-biopsied sites based on information from the biopsied sites. The details of this method are provided in the appendix. Briefly, this method considers the information from the biopsied sites as prior (represented by a beta distribution) and derives a posterior distribution using the Bayes theorem. The number of positive lesions among the non-biopsied sites is calculated from the implied beta-binomial distribution.

RESULTS

Patients

A total of 50 patients with progressive metastatic castrate-resistant prostate cancers were studied prospectively (Table S1). The protocol was approved by the Institutional Review Board of Memorial Sloan Kettering Cancer Center, the sole study site, and all patients provided signed informed consent. All patients underwent CT scan of chest, abdomen, and pelvis, as well as bone scintigraphy (MDP) within a month prior to imaging with ^{89}Zr-J591. In addition, all patients received an FDG PET/CT scan within two weeks prior to ^{89}Zr-J591 imaging. In two patients, an MRI of abdomen and pelvis was performed for clinical reasons and used for comparison of soft tissue findings (lesion in liver and a retroperitoneal node) and an additional two patients received a clinical MRI of the spine and femur, which was used for confirmation of bone lesion findings.

Administration of ^{89}Zr-J591 antibody was associated with infusion reactions in 16 patients, none of whom were premedicated. The reactions included grade I chills (n=12) and grade I chills with rigors (n=4). Three patients reported heavy breathing or shortness of breath and were treated with Benadryl 50 mg IV. In two of these patients, additional hydrocortisone 50 mg IV was administered. This is similar to our prior experience with the antibody (22, 23, 28, 29). No side effects were noted in patients who were premedicated.

Patient-based analysis

The distribution of lesions across bone, lymph nodes, and viscera are described in Table S1. ^{89}Zr-J591 antibody scans were positive in 44/50 patients for either bone and/or soft tissue lesions. Osseous lesions were seen in 29/50 patients with ^{89}Zr-J591as compared to 27/50 for bone scans. Visceral/ nodal disease was seen in 27/50 patients with ^{89}Zr-J591as

compared to 31/50 for CT scans. Of the 6 patients with negative ^{89}Zr-J591 scans, 4 had soft tissue or nodal disease seen on CT or FDG and 2/6 pts had bone lesions seen on MDP.

Analysis of bone lesions

A total of 439 lesions were detected by conventional imaging modalities, 392 of which were seen on ^{89}Zr-J591 (Table 1, Figure S2), resulting in a sensitivity of 89% (95% confidence interval: 85.5%-93.5%). These calculations follow the protocol definition of sensitivity and are also adjusted for clustering. MDP detected 339 lesions while ^{89}Zr-J591detected 491 sites. Of these, 302 sites were detected by both MDP and ^{89}Zr-J591 (89% concordance). ^{89}Zr-J591 showed 189 additional lesions in 23 patients that were not detected by MDP. MDP detected 37 lesions that were not detected by ^{89}Zr-J591 imaging. There was a linear relationship for the number of lesions detected by ^{89}Zr-J591scan versus MDP (Figure S1), with an estimated 34% higher detection rate for ^{89}Zr-J591 scan-positive lesions, across all of the patients. A total of 99 lesions were detected by ^{89}Zr-J591 imaging alone that were not seen by any other modality.

Lesions detected on ^{89}Zr-J591 imaging but not on MDP (J591+/MDP−)—There were 189 ^{89}Zr-J591+/MDP− lesions. Of these, 49 were also seen on FDG, another 35 showed stable sclerotic lesions on CT, and 64 other lesions were positive on follow-up MDP or FDG (obtained 1-6 months later with a median time of 4 months) (Figures 1 and S2). There were 41 lesions that were not confirmed to be metastatic prostate cancer within a follow-up time of 6 months; the impact of post-study treatment is unknown.

Lesions detected on MDP but not on ^{89}Zr-J591 imaging (J591−/MDP+)—A total of 37 sites were seen on MDP but not on ^{89}Zr-J591. Of these, 35 sites were also FDG-negative, while 2 were FDG-positive. The latter 2 sites (MDP-positive, FDG-positive, and ^{89}Zr-J591-negative) were biopsied and found to be negative for metastatic prostate cancer on histopathology (Figure 2). Of the 37 sites, 20 represented known sites of metastasis in correlation with other prior imaging with stable sclerosis on CT and exhibited increased uptake in the follow-up bone scan. An additional 8/37 sites were found to have benign etiology on follow-up imaging, while 9/37 remained stable on MDP and negative on FDG follow-up imaging.

Analysis of soft tissue

A total of 147 soft tissue lesions were identified by conventional imaging modalities, 73 of which were seen on ^{89}Zr-J591, resulting in a sensitivity of 50% (95% confidence interval: 39-61). ^{89}Zr-J591 imaging detected 90 soft tissue lesions in comparison to 124 soft tissue lesions detected by CT (Table 1). The lesions primarily included nodes; other soft tissue and organs included lung (n = 12), prostate bed (n = 4), liver (n = 3), adrenal (n = 2), seminal vesicle (n = 2), posterior bladder wall (n = 1), and brain lesion (n = 1). There were 65 (52%) concordant ^{89}Zr-J591 and CT-positive lesions; ^{89}Zr-J591 identified an additional 25 lesions (20%) not detected by CT scan, but was negative for 59 lesions detected by CT.

There were 43 concordant lesions between FDG and ^{89}Zr-J591, while ^{89}Zr-J591 identified an additional 47 lesions not detected by FDG. ^{89}Zr-J591 did not identify 45 lesions that were

positive on FDG. These lesions were predominantly mediastinal lymph nodes and lung nodules. Most of these lesions were sub-centimeter in size measuring 0.5-0.8 mm; 2 nodes measured 1.1 and 2.1 cm, and were close to the vasculature in the subaortic region or hilum. A total of 147 soft tissue lesions were seen by combined CT and FDG PET/CT imaging. In comparison to combined CT and FDG, ^{89}Zr-J591 showed 17 additional sites of disease.

Biopsy assessment

A total of 22 osseous sites (21 evaluatable) and 25 soft tissue sites were biopsied in 34 patients.

Bone lesions—There were 21 evaluable osseous sites; 19 were ^{89}Zr-J591-positive, whereas 2 sites were negative on ^{89}Zr-J591 imaging but had uptake on FDG PET (Table 2). Overall, 17/19 ^{89}Zr-J591-positive sites were also positive on pathology, while two sites were negative on pathology. One of these pathology-negative sites showed metastatic disease on MRI and a repeat biopsy performed clinically was positive for disease at this site. Thus, 18/19 (95%) osseous sites visible on ^{89}Zr-J591 PET imaging were considered true positives; 4 of these were seen only on ^{89}Zr-J591 imaging and had no correlate on other concurrent imaging modalities. Accordingly, 4 sites of occult disease were considered confirmed in bone (Figure 3). Two of the ^{89}Zr-J591-negative sites were biopsied; both were also negative for malignancy on pathology and follow-up. The overall accuracy in the biopsied osseous sites was 95.2% (21/22).

Soft tissue lesions—A total of 25 soft tissue lesions were biopsied, 22 of which were positive on pathology (Table 2). Of these 22, 14 ^{89}Zr-J591-positive (64%) and 8 ^{89}Zr-J591-negative sites (36%) were positive on pathology. CT was positive in 18/22 (84%) and FDG was positive in 13/22 (59%) of the biopsy-proven malignant lesions. There were 2 lesions that were positive on ^{89}Zr-J591 PET/CT but negative on pathology: one of these was adrenal gland uptake that was not suspicious on FDG and CT scan and was not positive on follow-up, while the second site was an external iliac node, which was also suspicious by FDG PET and CT scan. However, this site was benign on pathology and stable in FDG uptake and size on follow-up.

^{89}Zr-J591 imaging was negative for 8/22 pathologic positive sites, while FDG was negative for 9/22 sites. These 8/22 lesions were considered false negatives for ^{89}Zr-J591 imaging and included nodes, liver, and lung lesions that were otherwise seen on CT or FDG scan.

^{89}Zr-J591 lesion uptake: SUV comparison of bone and soft tissue lesions

Uptake was higher overall in the bone lesions than in the soft tissue lesions. The maximum SUV normalized for body weight (SUVmaxbw) for the bone lesions ranged from 1.35-37.2 with a median of 8.9. The SUVmaxbw for the nodal lesions ranged from 1.67-18.31 (median 4.8), and between 1.0-30.46 (median 4.8) for other soft tissue lesions. The difference between the SUVmax of bone lesions and all soft tissue lesions, including visceral and nodal disease, was statistically significant ($p < .001$). A comparison of SUV for soft tissue versus bone lesions within the same patient indicated that the uptake in bone lesions was independent of the uptake in soft tissue lesions, with no correlation observed. The SUV was

independent of lesion size, and the number of soft tissue or bone lesions in a patient was independent of each other, with no correlation seen in intra-patient analysis.

^{89}Zr-J591 lesion detection and PSA levels

The overall PSA range for these patients was 0.05-1,374 ng/mL (one patient had PSA of 1,374.6; otherwise, the maximum PSA level was 115.6 ng/mL). ^{89}Zr-J591 detected lesions in a patient with PSA as low as 0.23 ng/mL; in this patient, two bone lesions were detected, of which one was biopsy-proven for metastatic prostate disease. ^{89}Zr-J591 showed lesions in 6/8 patients with PSA < 1 ng/mL, (2 with bone lesions, 3 with nodal disease, and 1 with both soft tissue and bone lesions; see Figure S3) and an additional 10/11 patients with PSA below 2.5 ng/mL (6 with soft tissue lesions, 3 with bone lesions, and 1 with both bone and soft tissue lesions).

Predicted number of positive lesions among non-biopsied sites

We observed 439 bone and 147 soft tissue lesions with conventional imaging, providing precisions of +/− 3.5% and 11.5%, respectively, using the value of 0.1 for intra-class correlation. Using an emerging method of Bayesian analysis, we predicted the number of positive lesions among the non-biopsied sites for each modality separately for bone and soft tissue. The results, shown in Table 3, indicate that ^{89}Zr-J591 ranks the highest among all modalities in osseous tissue in terms of predicted number of positive findings (425, 95% posterior interval: 352-465), followed by bone scan (281, 220-314), CT (233, 176-270), and FDG (155, 116-180). In soft tissue lesions, CT had the highest number of predicted positives (86, 67-97), followed by ^{89}Zr-J591 (54, 40-64) and FDG (52, 37-61).

DISCUSSION

This is the first-in-human prospective phase I/II analytic validation study of a well characterized anti-PSMA antibody (J591) that uses ^{89}Zr-J591 PET for imaging metastatic prostate cancer. For comparators, we used a lesion multi-modality imaging comparison and biopsy data. We have previously reported the safety and biodistribution of ^{89}Zr-J591 in the first 10 patients in this cohort (26) and identified the optimal time for imaging with this intact antibody to be between day 6-8. We expanded the cohort to include an additional 40 patients with mCRPC to assess the ability of ^{89}Zr-J591 to accurately detect bone and soft tissue involvement in mCRPC. To our knowledge, this is the first comprehensive evaluation of anti-PSMA PET imaging in correlation with conventional imaging to evaluate its role as a biomarker.

^{89}Zr-J591 PET was superior for detecting bone metastases and bone lesions that were occult by the conventional imaging modalities of MDP, CT, and FDG. ^{89}Zr-J591 identified significantly more lesions compared to MDP, the most common modality for detecting bone metastasis in prostate cancer. Additionally, ^{89}Zr-J591 scans detected more skeletal lesions than FDG PET alone and combined findings on conventional imaging (Figure 3). A post-hoc analysis with follow-up imaging showed that about 75% of the additional lesions detected by ^{89}Zr-J591 subsequently became MDP-positive at the same site, and about 19% had stable sclerosis on CT scan. These findings suggest that ^{89}Zr-J591 targets PSMA

expression in viable disease that was not detected initially (MDP) or appeared stable (CT). The limitation of this interpretation is the assumption that a lesion seen in more than one modality is probably true disease. The visualization of the same sites on other imaging modalities at a later time may represent progression or, perhaps more likely, a difference in the ability to detect disease. We concluded that ^{89}Zr-J591imaging is able to detect viable disease earlier than conventional imaging. For lesions that were not initially seen on ^{89}Zr-J591 imaging compared to bone scan, most were non-hypermetabolic by FDG imaging with stable sclerosis on CT (site correlated). These tumor sites may represent inactive or treated disease.

Our study also confirmed ^{89}Zr-J591-positive sites by pathology to verify the finding of ^{89}Zr-J591 lesion uptake on a site-by-site basis, a critical component of this analysis. There was an overall high accuracy of ^{89}Zr-J591 lesion detection in correlation with pathology for bone metastasis. Although biopsy confirmation is ideal for establishing the presence of disease, there is a practical limitation of biopsying every (and sometimes, any) lesion seen on ^{89}Zr-J591 imaging. Because a majority of ^{89}Zr-J591-positive bony lesions were pathologically proven malignant, projections using Bayes' rule suggest that a large number (427/472) of non-biopsied bony sites are also likely true-positive sites, which would imply that the 170 of 189 additional sites seen by ^{89}Zr-J591 compared to MDP would be projected to be metastatic disease, as would 89/99 of the occult sites seen by ^{89}Zr-J591 compared to conventional imaging. This suggests that ^{89}Zr-J591 can likely detect occult sites of disease in advanced prostate cancer that otherwise went undetected—in this series, 50% more bone lesions than were detected by bone scan.

Based on the imaging analysis, biopsy results, and statistical projections, we conclude that ^{89}Zr-J591targeted imaging of PSMA is highly sensitive and accurate for bone disease with ≥ 90% probability that positive lesions are likely to represent true prostate cancer. By contrast, ^{89}Zr-J591 performed less well for the detection of soft tissue lesions, with an overall accuracy of 60%. ^{89}Zr-J591 PET in soft tissue sites clearly had lower uptake, with SUVmax < 50% of bone SUVs, and highly variable performance in soft tissue lesions overall. The detection of soft tissue lesions by ^{89}Zr-J591 (50% concordance with CIMs) was, however, similar to FDG imaging (47%). Few false-positive soft tissue lesions were detected by ^{89}Zr-J591, suggesting high specificity.

The lower detection rate of soft tissue disease may relate to generalized lower uptake. Additionally, the proximity of nodal lesions to vasculature, which retains activity for several days, limits the evaluation of nodal disease. Furthermore, other benign etiologies such as inflammation or granulomatous disease that were presumed as disease on CT and FDG scan may contribute to higher false-negative numbers noted for ^{89}Zr-J591. It is possible that the size of the intact antibody itself slows intra-tumoral penetration and may interfere with antibody binding and uptake in soft tissue metastases, or that the PSMA expression itself is lower in soft tissue disease than osseous metastases. Detailed molecular analysis is underway to evaluate these possibilities. The exact reason for overall lower uptake and detection of soft tissue lesions is not known at this time.

We recognize certain limitations of the study, as well as potential for bias. Most importantly, there is no single test that can serve as a gold standard for comparison. This constrains the assessment of the absolute total number of true lesions in a given patient. While a biopsy of every lesion is not practically possible given widespread skeletal disease in many patients, targeting the positive lesion introduces a bias toward assessment of the positive site only. Additionally, lesion detection may be limited by size and system resolution. For smaller lesions, about 250 mg in volume or less must have a substantial uptake of 5:1 to actually be seen (30). The treatment received by patients following the imaging was variable, which limited the assessment of lesions through follow-up imaging.

^{89}Zr-J591 PET imaging also presents some practical limitations. Due to the larger size of the antibody leading to the long blood clearance time, 6-8 days are required for optimal tumor visualization, post-injection. The hepatic and renal uptake is considerable, which interferes with the detection of rare metastases to these organs. Dosimetry to these organs limits the dose of injected activity and later imaging requires longer duration. The assessment of soft tissue disease appears less optimal. Given these limitations, smaller molecular agents directed to PSMA that have faster clearance and show lesions earlier may be more suitable for assessment. We are now exploring the use of an anti-PSMA minibody derived from J591 (31) for the detection of early changes in bone disease in advanced prostate cancer and assessment of treatment response in castration-resistant prostate cancer.

Supplementary Material

Refer to Web version on PubMed Central for supplementary material.

ACKNOWLEDGMENTS

The authors thank the research study assistants, clinical research coordinators, research managers, research nurses, technologists, and radiopharmacists for making this study possible. The authors also thank Leah Bassity for her editorial assistance.

Financial support: This study was funded by Starr Cancer Consortium, the prostate cancer program of Memorial Sloan Kettering Cancer Center, the Center for Targeted Radioimmunotherapy and Theranostics of the Ludwig Center for Cancer Immunotherapy, and the David H. Koch Foundation. In addition, the Radiochemistry & Molecular Imaging Probes Core of MSK is supported in part by NIH P30CA008748, the Landy Research Fund, and Hascoe Charitable Foundation.

APPENDIX

Imaging studies of metastatic prostate cancer are challenged by the presence of large numbers of lesions, of which only a small number can be biopsied. This precludes the use of traditional metrics of diagnostic accuracy such as sensitivity and specific and predictive value. To partially remedy this, we have used a Bayesian approach to use the information in biopsied lesions and project the number of cancerous lesions among the non-biopsied sites. This approach relies on the Bayes theorem to calculate conditional probabilities. It entails using the proportions of cancerous sites as “prior” information and applying the Bayes theorem to calculate the conditional expectation of the number of cancerous lesions among the non-biopsied sites given (conditional on) what has been revealed in the biopsied sites.

To formalize this line of thinking, we denote by θ the probability that a lesion identified radiographically is cancerous. This is conceptually similar to the positive predictive value. Prior to observing the biopsy data, we have no information on θ other than that it must be between 0 and 1. This can be represented by the uniform distribution, also known as a beta distribution, with parameters 1 and 1 (Figure A1).

Using as an example the J591 imaging of osseous tissue, 18 of the 19 J591-positive sites were biopsy-positive, which translates the above uniform distribution to the one depicted in Figure A2. This is a beta distribution with parameters 19 and 2. These parameters are found by adding the parameters of the uniform distribution to the number of positive and negative sites among the biopsied ones. Notice that this distribution appropriately reflects the change in the way we see θ after observing a high rate of positivity among the biopsied sites. Values below 0.6 are considered extremely unlikely and the distribution peaks around 0.95. We can make these calculations very precise; the probability that $\theta < 0.6$ is 0.0005 and the expected value is (18+1)/(19+2) = 0.905, which is our best estimate for the probability that a J591-positive lesion will be biopsy-positive. But it also reflects the remaining uncertainty due to the relatively small number of sites biopsied, e.g., the probability that $\theta < 0.9$ is 0.392, a substantial amount.

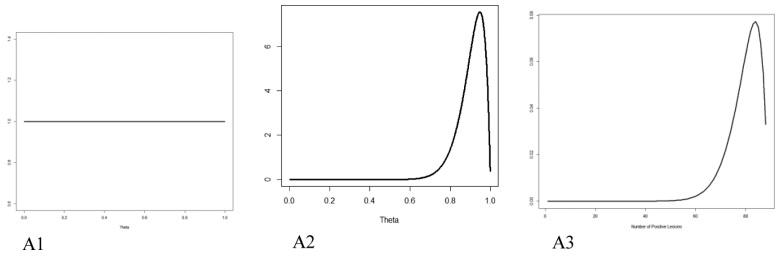

Figure A.
Uniform prior distribution (A1); beta (19, 2) distribution for the probability that a J591-positive site will be biopsy-positive, which reflects the information gleaned from the biopsied sites (A2); and beta-binomial (470, 19, 2) distribution for the number of biopsy-positive lesions among the non-biopsied J591-positive lesions (A3).

This distribution also allows us to project the number of positives in a given number of non-biopsied sites. The distribution of the number of positive sites is called beta-binomial with parameters; in this case, 470 (the number of non-biopsied sites) and 19 and 2 (same parameters as the beta distribution). Various probabilities of interest can be calculated from here. There is virtually no chance (1.2%) that fewer than 350 lesions will be positive. The expected (mean) number of positive lesions is 442, with a confidence interval of 366-484. When added to the 18 positive lesions from biopsied sites, this implies a total of 460 positive lesions (confidence interval of 378-491). The interpretation of this interval is more intuitive than a classical confidence interval, due to its Bayesian nature: the probability that the number of positive lesions is between 378 and 491 is 0.95.

REFERENCES

1. Jadvar H, Desai B, Ji L, Conti PS, Dorff TB, Groshen SG, et al. Baseline 18F-FDG PET/CT parameters as imaging biomarkers of overall survival in castrate-resistant metastatic prostate cancer. J Nucl Med. 2013; 54(8):1195–201. [PubMed: 23785174]
2. Yu EY, Muzi M, Hackenbracht JA, Rezvani BB, Link JM, Montgomery RB, et al. C11-acetate and F-18 FDG PET for men with prostate cancer bone metastases: relative findings and response to therapy. Clin Nucl Med. 2011; 36(3):192–8. [PubMed: 21285676]
3. Sengoku T, Matsumura K, Usami M, Takahashi Y, Nakayama T. Diagnostic accuracy of FDG PET cancer screening in asymptomatic individuals: use of record linkage from the Osaka Cancer Registry. Int J Clin Oncol. 2014; 19(6):989–97. [PubMed: 24481919]
4. Minamimoto R, Uemura H, Sano F, Terao H, Nagashima Y, Yamanaka S, et al. The potential of FDG-PET/CT for detecting prostate cancer in patients with an elevated serum PSA level. Ann Nucl Med. 2011; 25(1):21–7. [PubMed: 20931305]
5. Morris MJ, Akhurst T, Larson SM, Ditullio M, Chu E, Siedlecki K, et al. Fluorodeoxyglucose positron emission tomography as an outcome measure for castrate metastatic prostate cancer treated with antimicrotubule chemotherapy. Clin Cancer Res. 2005; 11(9):3210–6. [PubMed: 15867215]
6. Meirelles GS, Schoder H, Ravizzini GC, Gonen M, Fox JJ, Humm J, et al. Prognostic value of baseline [18F] fluorodeoxyglucose positron emission tomography and 99mTc-MDP bone scan in progressing metastatic prostate cancer. Clin Cancer Res. 2010; 16(24):6093–9. [PubMed: 20975102]
7. Murphy GP, Elgamal AA, Su SL, Bostwick DG, Holmes EH. Current evaluation of the tissue localization and diagnostic utility of prostate specific membrane antigen. Cancer. 1998; 83(11): 2259–69. [PubMed: 9840525]
8. Bostwick DG, Pacelli A, Blute M, Roche P, Murphy GP. Prostate specific membrane antigen expression in prostatic intraepithelial neoplasia and adenocarcinoma: a study of 184 cases. Cancer. 1998; 82(11):2256–61. [PubMed: 9610707]
9. McCarthy M, Siew T, Campbell A, Lenzo N, Spry N, Vivian J, et al. (1)(8)F Fluoromethylcholine (FCH) PET imaging in patients with castration-resistant prostate cancer: prospective comparison with standard imaging. Eur J Nucl Med Mol Imag. 2011; 38(1):14–22.
10. Ceci F, Castellucci P, Graziani T, Schiavina R, Brunocilla E, Mazzarotto R, et al. (11)C Choline PET/CT detects the site of relapse in the majority of prostate cancer patients showing biochemical recurrence after EBRT. Eur J Nucl Med Mol Imag. 2014; 41(5):878–86.
11. Picchio M, Spinapolice EG, Fallanca F, Crivellaro C, Giovacchini G, Gianolli L, et al. [11C]Choline PET/CT detection of bone metastases in patients with PSA progression after primary treatment for prostate cancer: comparison with bone scintigraphy. Eur J Nucl Med Mol Imag. 2012; 39(1):13–26.
12. Rodari M, Lopci E, Pepe G, Antunovic L, Chiti A. [11C]-choline PET/CT in imaging locally advanced prostate cancer. Nucl Med Rev Cent E Eur. 2011; 14(2):118–9.
13. Haseebuddin M, Dehdashti F, Siegel BA, Liu J, Roth EB, Nepple KG, et al. 11C-acetate PET/CT before radical prostatectomy: nodal staging and treatment failure prediction. J Nucl Med. 2013; 54(5):699–706. [PubMed: 23471311]
14. Beheshti M, Imamovic L, Broinger G, Vali R, Waldenberger P, Stoiber F, et al. 18F choline PET/CT in the preoperative staging of prostate cancer in patients with intermediate or high risk of extracapsular disease: a prospective study of 130 patients. Radiology. 2010; 254(3):925–33. [PubMed: 20177103]
15. Larson SM, Morris M, Gunther I, Beattie B, Humm JL, Akhurst TA, et al. Tumor localization of 16beta-18F-fluoro-5alpha-dihydrotestosterone versus 18F-FDG in patients with progressive, metastatic prostate cancer. J Nucl Med. 2004; 45(3):366–73. [PubMed: 15001675]
16. Afshar-Oromieh A, Zechmann CM, Malcher A, Eder M, Eisenhut M, Linhart HG, et al. Comparison of PET imaging with a (68)Ga-labelled PSMA ligand and (18)F-choline-based PET/CT for the diagnosis of recurrent prostate cancer. Eur J Nucl Med Mol Imag. 2014; 41(1):11–20.

17. Hamilton A, King S, Liu H, Moy P, Bander N, Carr F. A novel humanised antibody against prostate specific membrane antigen (PSMA) for in vivo targeting and therapy. Proc Am Assoc Cancer Res Ann Mtg. 1998; 39:440.
18. Bander NH, Trabulsi EJ, Kostakoglu L, Yao D, Vallabhajosula S, Smith-Jones P, et al. Targeting metastatic prostate cancer with radiolabeled monoclonal antibody J591 to the extracellular domain of prostate specific membrane antigen. J Urol. 2003; 170(5):1717–21. [PubMed: 14532761]
19. Bander NH, Nanus DM, Milowsky MI, Kostakoglu L, Vallabahajosula S, Goldsmith SJ. Targeted systemic therapy of prostate cancer with a monoclonal antibody to prostate-specific membrane antigen. Sem Oncol. 2003; 30(5):667–77.
20. Bander NH, Nanus D, Bremer S, Smith-Jones P, Kostakoglu L, Vallabhajosula S, et al. Phase 1 clinical trial targeting a monoclonal antibody (mAb) to the extracellular domain of prostate specific membrane antigen (PSMAext) in hormone-independent patients. J Urol. 2000; 163(4 Suppl.):160.
21. Pandit-Taskar N, O'Donoghue JA, Morris MJ, Wills EA, Schwartz LH, Gonen M, et al. Antibody mass escalation study in patients with castration-resistant prostate cancer using (111)In-J591: Lesion detectability and dosimetric projections for (90)Y Radioimmunotherapy. J Nucl Med. 2008; 49(7):1066–74. [PubMed: 18552139]
22. Morris MJ, Pandit-Taskar N, Divgi CR, Bender S, O'Donoghue JA, Nacca A, et al. Phase I evaluation of J591 as a vascular targeting agent in progressive solid tumors. Clin Cancer Res. 2007; 13(9):2707–13. [PubMed: 17473203]
23. Morris MJ, Divgi CR, Pandit-Taskar N, Batraki M, Warren N, Nacca A, et al. Pilot trial of unlabeled and indium-111-labeled anti-prostate-specific membrane antigen antibody J591 for castrate metastatic prostate cancer. Clin Cancer Res. 2005; 11(20):7454–61. [PubMed: 16243819]
24. Vallabhajosula S, Kostakoglu L, Hamacher KA, Brandman S, Bander NH, Goldsmith SJ. Pharmacokinetics, biodistribution and radiation dosimetry of radiolabeled anti-PSMA antibody: comparison of In-111-DOTA-J591 with Lu-177-dota-J591. J Nucl Med. 2003; 44(5):322P–P.
25. Holland JP, Divilov V, Bander NH, Smith-Jones PM, Larson SM, Lewis JS. Zr-89-DFO-J591 for immunoPET of prostate-specific membrane antigen expression in vivo. J Nucl Med. 2010; 51(8): 1293–300. [PubMed: 20660376]
26. Pandit-Taskar N, O'Donoghue JA, Beylergil V, Lyashchenko S, Ruan S, Solomon SB, et al. 89Zr-huJ591 immuno-PET imaging in patients with advanced metastatic prostate cancer. Eur J Nucl Med Mol Imag. 2014; 41(11):2093–105.
27. Vosjan MJ, Perk LR, Visser GW, Budde M, Jurek P, Kiefer GE, et al. Conjugation and radiolabeling of monoclonal antibodies with zirconium-89 for PET imaging using the bifunctional chelate p-isothiocyanatobenzyl-desferrioxamine. Nature Protocols. 2010; 5(4):739–43. [PubMed: 20360768]
28. Milowsky MI, Nanus DM, Kostakoglu L, Sheehan CE, Vallabhajosula S, Goldsmith SJ, et al. Vascular targeted therapy with anti-prostate-specific membrane antigen monoclonal antibody J591 in advanced solid tumors. Journal of Clinical Oncology. 2007; 25(5):540–7. [PubMed: 17290063]
29. Milowsky MI, Nanus DM, Kostakoglu L, Vallabhajosula S, Goldsmith SJ, Bander NH. Phase I trial of yttrium-90-labeled anti-prostate-specific membrane antigen monoclonal antibody J591 for androgen-independent prostate cancer. Journal of Clinical Oncology. 2004; 22(13):2522–31. [PubMed: 15173215]
30. Erdi YE. Limits of tumor detectability in nuclear medicine and PET. Mol Imag Radionucl Ther. 2012; 21(1):23–8.
31. Viola-Villegas NT, Sevak KK, Carlin SD, Doran MG, Evans HW, Bartlett DW, et al. Noninvasive imaging of PSMA in prostate tumors with (89)Zr-labeled huJ591 engineered antibody fragments: the faster alternatives. Mol Pharmaceutics. 2014; 11(11):3965–73.

STATEMENT OF TRANSLATIONAL RELEVANCE

An imaging biomarker that accurately detects active metastatic disease, particularly in bone, will likely play a critical role in the management of advanced prostate cancer and selection of patients for optimal therapy. We studied ^{89}Zr-J591, a radiolabeled antibody targeting prostate-specific membrane antigen (PSMA) using PET imaging, and showed superior targeting of bone lesions relative to any standard imaging modality or combination of standard imaging modalities. This study establishes a benchmark to assess the effectiveness of alternative prostate cancer imaging biomarkers, including those targeting PSMA, such as radiolabeled minibody (IAB2M) or urea-based small peptides.

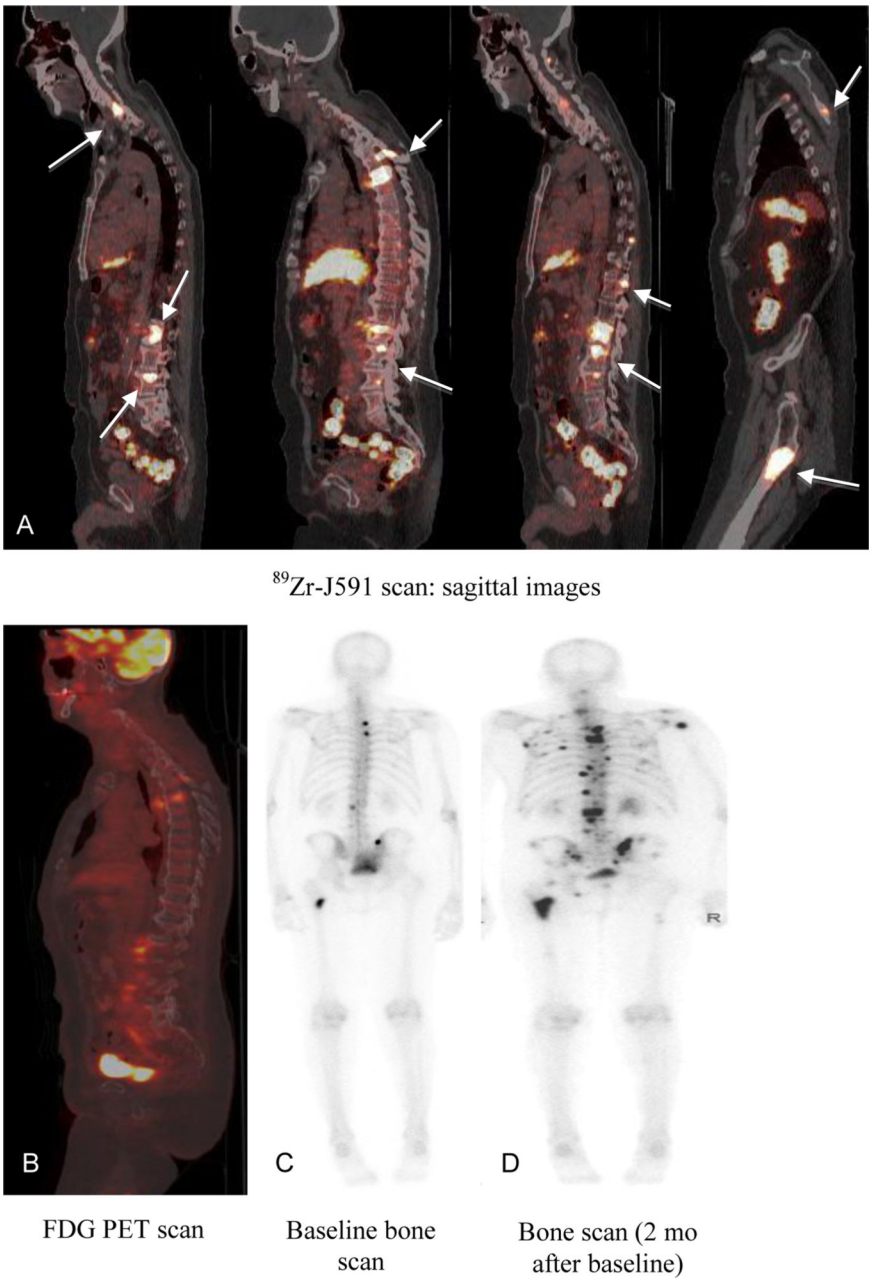

Figure 1.

Patient with metastatic prostate cancer (PSA 90.9) with ^{89}Zr-J591-positive lesions that were not seen on MDP. Follow-up imaging showed POD on MDP. ^{89}Zr-J591 scan (A) showed uptake in multiple bone sites (arrows) that were not seen on concurrent FDG scan (B) or bone scan (C). A follow-up bone scan (D) showed uptake in the sites and was consistent with POD.

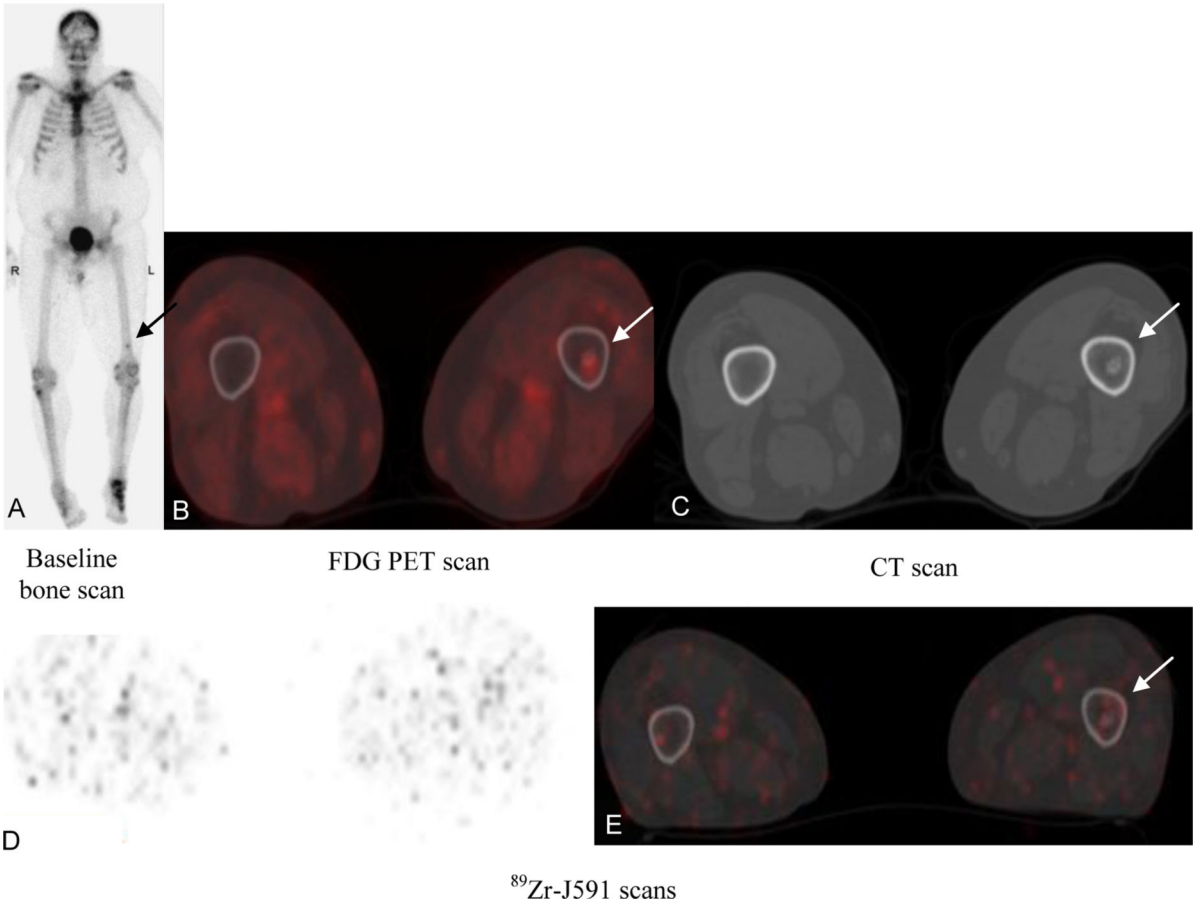

Figure 2.

Patient with metastatic prostate cancer (PSA of 27.4). Baseline bone scan (A) and FDG PET (B) showed suspicious uptake in left femur distally (arrow); CT scan (C) showed sclerotic focus in the region. ^{89}Zr-J591 scan transaxial and fused images (D, E) did not show any suspicious uptake. Biopsy of the femoral lesion showed benign enchondroma.

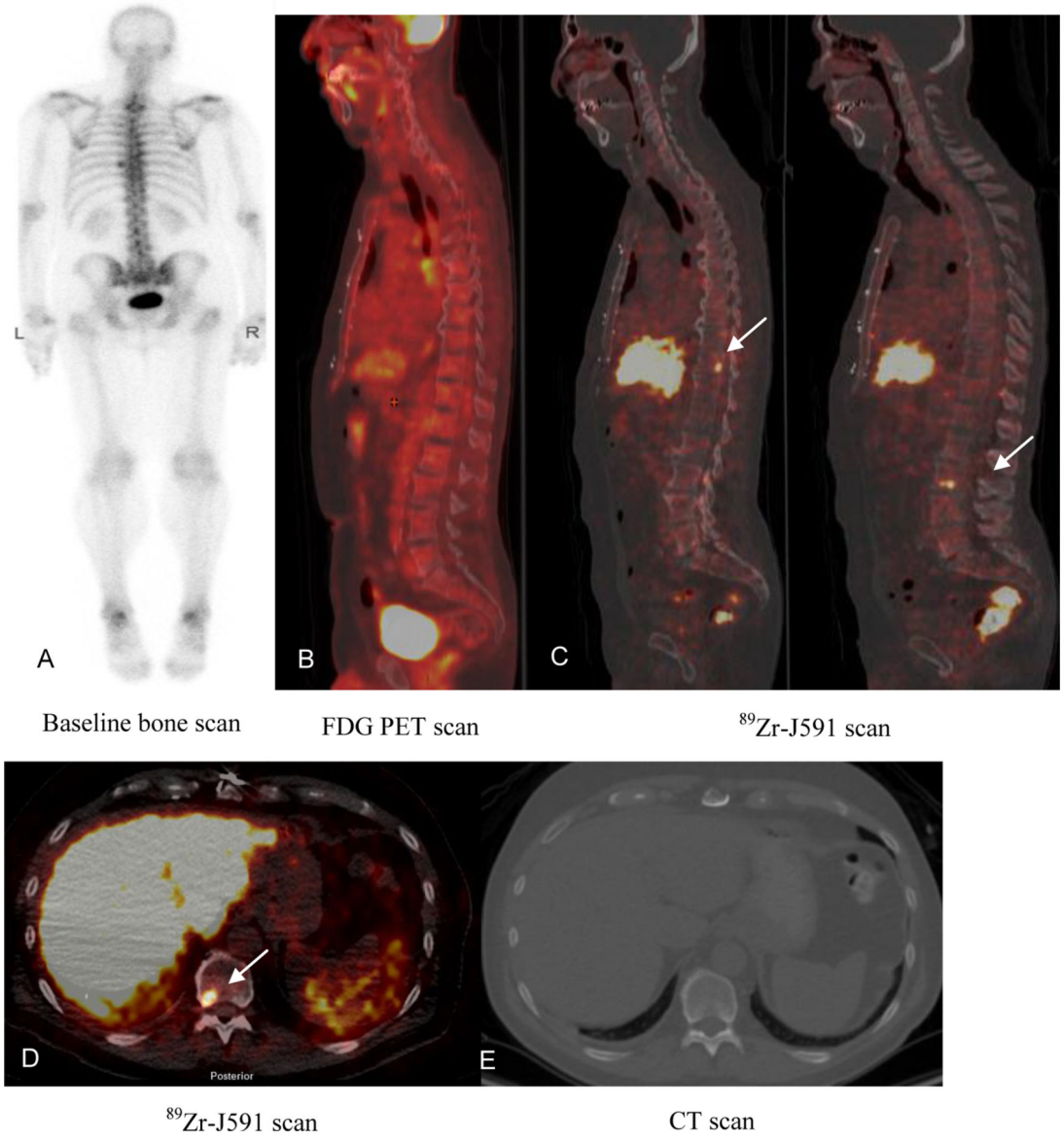

Figure 3.

Patient with metastatic prostate cancer (PSA of 4.1). Baseline bone scan (A) and FDG PET (B) showed no suspicious lesions. ^{89}Zr-J591 scan (C) showed uptake in T11 and L3 as seen on sagittal images (C) and transaxial image (D) (arrows). CT scan did not show any corresponding abnormality (E). Biopsy of T11 was positive for metastatic carcinoma.

Table 1

Bone and soft tissue lesions: Comparative lesion detection by imaging modality

Bone lesions

	MDP+	MDP-	FDG+	FDG-	CT+	CT-	CIM+	CIM-	TOTAL
Zr-J591+	302	189	202	289	281	210	392	99	**491**
Zr-J591-	37	10	5	42	20	27	47	NA	
TOTAL	**339**	**199**	**207**	**331**	**301**	**237**	**439**	**99**	

Soft tissue lesions

	FDG+	FDG-	CT+	CT-	CIM+	CIM-	TOTAL
Zr-J591+	43	47	65	25	73	17	**90**
Zr-J591-	45	29	59	15	74	NA	
TOTAL	**88**	**76**	**124**	**40**	**147**	**17**	

Legend: MDP, methylenediphosphonate bone scan; FDG, F-flourodeoxyglucose; CT, computerized tomography; CIM, conventional imaging modalities; Zr-J591, ^{89}Zr-DFO-huJ591

Table 2

Biopsy correlation with imaging

Bone lesions						
	J591+	**J591-**	**MDP+**	**MDP-**	**FDG+**	**FDG-**
Biopsy-positive (n=18)	18*	0	14	4	14	4
Biopsy-negative (n=3)	1	2	1	2	2	1

Soft tissue lesions						
	J591+	**J591-**	**CT+**	**CT-**	**FDG+**	**FDG-**
Biopsy-positive (n=22)	14	8	18	4	13	9
Biopsy-negative (n=3)	2	1	1	2	2	1

Legend: J591, ^{89}Zr-DFO-huJ591; MDP, methylenediphosphonate bone scan; FDG, ^{18}F-fluorodeoxyglucose; CT, computerized tomography

* One site was originally negative on pathology, but showed progression on follow-up imaging; a repeat biopsy (performed clinically) was positive for metastatic disease.

Table 3

Bayesian prediction for disease in visualized lesions

Modality	Tissue	Sites + on scans	Total sites biopsied	Total pathology + lesions	Number of scan+ sites biopsied	Scan+ & biopsy+	Non-biopsied, scan+ sites	Estimated biopsy+ sites of non-biopsied scan+ group	95% CI
J591	Bone	491	21	^{18}*	19	^{18}*	470	425	352-465
BS	Bone	339	21	^{18}*	15	14	318	281	220-314
CT	Bone	301	21	^{18}*	16	14	280	233	176-270
FDG	Bone	207	21	^{18}*	16	14	186	155	116-180
CT	Soft	124	25	22	20	18	99	86	67-97
J591	Soft	90	25	22	16	14	65	54	40-64
FDG	Soft	88	25	22	15	13	63	52	37-61

* Note: One site was originally negative on pathology, but showed progression on follow-up imaging; a repeat biopsy (performed clinically) was positive for metastatic disease.